

Three-dimensional wake transition in the flow over four square cylinders at low Reynolds numbers

Cite as: AIP Advances **10**, 015142 (2020); <https://doi.org/10.1063/1.5129744>

Submitted: 01 October 2019 • Accepted: 05 January 2020 • Published Online: 22 January 2020

Yuhang Zhang, Rui Wang, Yaoran Chen, et al.



View Online



Export Citation



CrossMark

ARTICLES YOU MAY BE INTERESTED IN

[Dynamic response of a cable with triangular cross section subject to uniform flow at Reynolds number 3900](#)

[Physics of Fluids](#) **32**, 045103 (2020); <https://doi.org/10.1063/1.5144402>

[Turbulent wake suppression of circular cylinder flow by two small counter-rotating rods](#)

[Physics of Fluids](#) **32**, 115123 (2020); <https://doi.org/10.1063/5.0023881>

[Transition to chaos in the wake of a circular cylinder near a moving wall at low Reynolds numbers](#)

[Physics of Fluids](#) **32**, 091703 (2020); <https://doi.org/10.1063/5.0022560>

READ NOW!

AIP Advances

Energy Collection

Three-dimensional wake transition in the flow over four square cylinders at low Reynolds numbers

Cite as: AIP Advances 10, 015142 (2020); doi: 10.1063/1.5129744

Submitted: 1 October 2019 • Accepted: 5 January 2020 •

Published Online: 22 January 2020



Yuhang Zhang,¹ Rui Wang,¹ Yaoran Chen,¹ Yan Bao,¹ Zhaolong Han,^{1,2,3,a)} Dai Zhou,^{1,2,3,b)} Huan Ping,¹ Shixiao Fu,^{1,2,3} and Yongsheng Zhao^{1,3}

AFFILIATIONS

¹School of Naval Architecture, Ocean and Civil Engineering, Shanghai Jiao Tong University, Shanghai 200240, China

²Key Laboratory of Hydrodynamics of Ministry of Education, Minhang Campus, Shanghai 200240, People's Republic of China

³State Key Laboratory of Ocean Engineering, Shanghai Jiao Tong University, Shanghai 200240, China

^{a)}Author to whom correspondence should be addressed: han.arkey@sjtu.edu.cn

^{b)}Electronic mail: zhoudai@sjtu.edu.cn

ABSTRACT

The three-dimensional characteristics of the flow past four square cylinders in an in-line square configuration, with five spacing ratios ranging from 1.4 to 5, were studied in depth in this study. Direct numerical simulation of the spectral/hp element method was employed at $Re = 150$ and 200. The onset and evolution of various unstable modes were expounded in detail by means of three-dimensional vortices, energy curves, wake patterns, and force coefficients. At each spacing, the three-dimensional instability and the corresponding flow pattern were comprehensively analyzed to illustrate transitional features. Except for the existence of unstable mode A and mode B when spacing was considerably small and large, for most of the intermediate spacing ratios, the vortex structures were dominated by mode C instability, whose flow patterns all appeared as anti-phase synchronization. Through the evolution of flow patterns over time, the three-dimensional effects were already observed at a low Reynolds number of 150 because of the influence of the gap flow and the mutual interference of the wake. Under the transitional spacing for $Re = 200$, multiple modes were interfering fiercely with each other and appeared as chaotic states. Compared with other bluff body forms, the four square cylinders generated numerous discrepancies and new modal transitions in three-dimensional cases.

© 2020 Author(s). All article content, except where otherwise noted, is licensed under a Creative Commons Attribution (CC BY) license (<http://creativecommons.org/licenses/by/4.0/>). <https://doi.org/10.1063/1.5129744>

I. INTRODUCTION

Flow over bluff bodies has been widely studied due to its practical and scientific significance. The related wake flow comprises rich complex physical phenomena, such as the separated shear layer, vortex shedding, and three-dimensionalization. In order to understand the intrinsic mechanism of fluid dynamics, numerous investigations have been performed to study the onset and evolution of the three-dimensionality of wake flow, experimentally,^{1,2} analytically,³ and numerically.⁴

The three-dimensional wake transition of a circular cylinder (CC) was first experimentally investigated by Williamson.^{2,5} He identified two successive three-dimensional transitions: mode A,

where the first three-dimensional unstable mode was accompanied by the generation of large-scale vortex (mode A*), appearing at $Re \approx 180$ –194, which is characterized by the spanwise wavelength of $4D$; and mode B, appearing at $Re \approx 230$ –260 with a spanwise wavelength of about $0.8D$. These results were confirmed by the numerical work of Barkley and Henderson,³ who conducted a highly accurate Floquet stability analysis to determine the critical Re values of modes A and B. Using the same method, Robichaux *et al.*⁶ examined the three-dimensional instabilities in the wake of a square cylinder. It was found that the physical mechanism of the two fundamental unstable modes for a square cylinder (SC) is generally consistent with those for a circular cylinder. The discrepancy was that mode A was observed to become unstable at a Reynolds number of 161,

with a critical spanwise wavelength of about $5D$, while mode B was observed to become unstable at a Reynolds number of 190, with a critical spanwise wavelength of about $1.1D$. In curves of neutral stability, the wavelength corresponding to the critical Reynolds number is the critical spanwise wavelength. They also detected an intermediate-wavelength subharmonic mode (mode S), which was actually found to be a quasiperiodic mode (mode QP) by Blackburn and Lopez.⁷ Williamson^{2,5} explained that mode A is stemmed from the elliptic instability of the near-wake vortex core, while the hyperbolic instability of the braid shear layers is the main reason for mode B.

Sub-harmonic mode C, with twice the shedding period of the two-dimensional base flow, was first found by Zhang *et al.*,⁸ by using a thin wire closed to a circular cylinder. It was revealed that the mode C instability has a distinct structure from modes A and B. Later, mode C was also observed in the wake of a ring⁹ and the inclined square cylinder.¹⁰ Mode C results from the subharmonic mechanism, as proposed by Sheard *et al.*¹¹

As the bluff body system can present different profiles and arrangements, the fluid mechanics of three-dimensional transition may vary for different structural forms, for instance, in the wake transitions of two circular cylinders in staggered¹² or tandem¹³ arrangements. Compared with the circular cylinder, the geometrical characteristics of the multiple square cylinders may make it have a different transition process. Choi and Yang,¹⁴ and Choi *et al.*¹⁵ studied two square cylinders in tandem and side-by-side arrangements via Floquet stability analysis. The main spanwise wavelength for each pattern was presented. At the same time, the three-dimensional instability modes corresponding to multiple flow patterns generated under different gaps were summarized. In addition, there were new flow characteristics as the number of square cylinders continuously increased.

For four circular cylinders in square arrangement, related studies have become exceedingly abundant in recent years. Lam *et al.*^{16,17} experimentally investigated the flow over four circular cylinders in a square configuration. It was concluded that the flow characteristics can be divided into three direct flow patterns at different spacing ratio intervals. The influences of different spacing on force coefficients and pressure distribution at the critical Reynolds number were revealed by Lam and Zou.¹⁸ The numerical simulation was conducted to study the flow field characteristics shown by Lam *et al.*,¹⁹ and it was found that the two-dimensional simulation results were quite different from the experimental data under some specific Reynolds numbers around four cylinders, and the three-dimensional simulation could better fit the experimental data to reveal the pivotal role of the three-dimensional effects. Thereafter, Lam and Zou²⁰ investigated the influences of spacing ratio (L/D) and aspect ratio (H/D) on three-dimensional flow characteristics around four circular cylinders at a Reynolds number of 200, as well as the features of force and pressure coefficients on the cylinders. Tong *et al.*²¹ have investigated the vortex shedding regime with Reynolds number as a variable and the hydrodynamic characteristics on four circular cylinders by fixed spacing. Furthermore, two different flow incidence angles were adopted to study the wake characteristics.²² The above major contents in regard to the four circular cylinders were mainly focusing on the hydrodynamic characteristics and wake flow regimes. There was little research on the transition of unstable modes.

Multi-cylinder groups are common in engineering practice. For flow past side-by-side bluff body structure, the two shear layers will interact with each other, which will generate a new wake mode. For flow past structures in tandem arrangement, the vortex shedding from the upstream bluff body impacts the downstream structure, which will change the overall wake characteristics. The four-cylinder structure satisfies both of the above arrangements. In the available literature, the flow past four circular cylinders has been extensively investigated, and many new wake characteristics have been found. However, for four square cylinder configuration, considering that the structure has sharp edges, it will have a huge impact on the separation of the fluid and the shedding of the vortex. The offshore platforms and building group in the actual engineering have the structure of square cylinders, and there is no investigation on this configuration. The study on flow past four square cylinders is of great significance. In order to fill this gap, the goal of the present paper is to use the three-dimensional direct numerical simulations to investigate the three-dimensionalization of the wake, as well as the evolution of the three-dimensional instabilities for different geometrical configurations.

This paper is organized as follows. In Sec. II, the physical models are described and the numerical methods utilized in the simulations are demonstrated and validated. Then, the detailed numerical results are presented and explained in Sec. III. Finally, Sec. IV contains the key conclusions, summarizing the main findings of the present study.

II. PHYSICAL MODEL AND NUMERICAL METHODOLOGY

A. Physical model

Figure 1 illustrates a schematic of the geometrical configuration in this work. Four identical square cylinders in an inline square arrangement are considered, where SC is an abbreviation of square cylinder and CC of circular cylinder in subsequent figures and tables. The side length of the square cylinder is defined as D and the center-to-center spacing of two square cylinders is defined as L . The upstream and downstream boundaries are, respectively, located at $32D$ and $52D$ from the center of the four-square-cylinder system, and the two lateral boundaries are located $32D$ from the center of the four-square-cylinder system. Five different spacing ratios in the

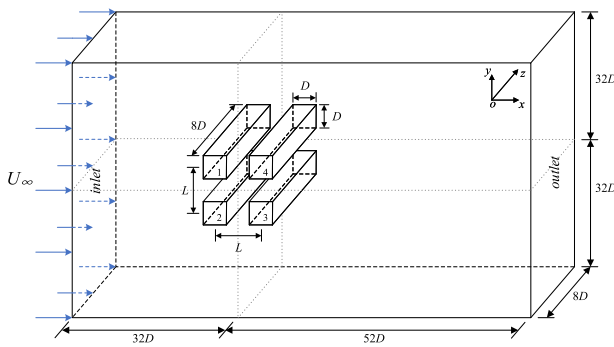


FIG. 1. Schematic view of the flow past the four square cylinders.

range from 1.4 to 5 are considered in this study, i.e., $L/D = 1.4, 2.5, 3.5, 4$, and 5 . The Reynolds number is defined based on the free-stream U_∞ and the side length D , i.e., $Re = U_\infty D/v$, where v is the kinematic viscosity. Two Reynolds numbers of 150 and 200 are selected. The principal objective of this study is to explore how the three-dimensionality of the wake develops as the spacing ratio and the Reynolds number alter.

B. Numerical methodology

The three-dimensional Navier–Stokes equations for incompressible viscous flow can be expressed in the vector form as

$$\frac{\partial \mathbf{u}}{\partial t} = -(\mathbf{u} \cdot \nabla) \mathbf{u} - \nabla p + \frac{1}{Re} \nabla^2 \mathbf{u}, \quad (1)$$

$$\nabla \cdot \mathbf{u} = 0, \quad (2)$$

where $\mathbf{u} = (u, v, w)$ is the velocity vector, t is the time, and p is the pressure. The above equations are resolved by employing the parallel Fourier spectral/hp element method²³ embedded in open-source code Nektar++ (Cantwell *et al.*²⁴ and Xu *et al.*²⁵), in which a three-step time-splitting scheme is used, allowing primitive variables to be processed independently in each time step.^{26,27} The spanwise wavenumbers of the three-dimensional flow vortices can be obtained by Fourier expansion. This solver has widely been validated and used to investigate the flow over bluff bodies (Jiang *et al.*,²⁸ Rocco and Sherwin,²⁹ Tong *et al.*,³⁰ Wang *et al.*,³¹ and Yan *et al.*³²). A precise development of the flow field can be obtained by direct numerical simulation.

Based on the assumption that the flow variable is uniform in the spanwise direction, Fourier expansion is introduced into the flow variables \mathbf{u} and p in the z direction as

$$\mathbf{u}(x, y, z, t) = \sum_{m=0}^{M-1} \mathbf{u}_m(x, y, t) e^{i\beta mz}, \quad p(x, y, z, t) = \sum_{m=0}^{M-1} p_m(x, y, t) e^{i\beta mz}, \quad (3)$$

where m is the Fourier mode index and M is the number of modes in the Fourier expansion. Here, $\beta = 2\pi/L_z$, where L_z represents the

periodic length. When Eqs. (1) and (2) are applied in the Fourier transformation, a series of uncoupled two-dimensional equations are obtained for each mode,³³

$$\frac{\partial u_m}{\partial t} + \widehat{N(\mathbf{u})}_m = -\widetilde{\nabla} p_m + v \widetilde{\nabla}^2 \mathbf{u}_m, \quad (4)$$

$$\widetilde{\nabla} \cdot \mathbf{u}_m = 0, \quad (5)$$

where $\widehat{N(\mathbf{u})}_m$ is the Fourier mode of the convective term. The Fourier transformation of nonlinear terms is applied to the physical space to eliminate the influences of convolution sums. The differential operators in Eqs. (4) and (5) are defined as

$$\widetilde{\nabla} = \left(\frac{\partial}{\partial x}, \frac{\partial}{\partial y}, i\beta m \right), \quad \widetilde{\nabla}^2 = \frac{\partial^2}{\partial x^2} + \frac{\partial^2}{\partial y^2} - \beta^2 m^2. \quad (6)$$

Note that for the three-dimensional simulations, with the homogeneous spanwise direction being treated using a Fourier expansion in the discretization, only two-dimensional mesh is required. An example of the two-dimensional meshes utilized in the present study is shown in Fig. 2 for the case of $L/D = 2.5$. The boundary conditions are specified as follows: at the inlet and the two lateral boundaries, a uniform free-stream velocity ($u = 1, v = 0$) is specified; at the outlet, the Neumann boundary conditions ($\frac{\partial u}{\partial n} = 0, \frac{\partial v}{\partial n} = 0$) are enforced; on the square cylinder surface, a no-slip condition ($u = 0, v = 0$) is imposed; for pressure, a high-order Neumann condition is set at the inlet and lateral boundaries, while it is set to zero at the outlet.²⁶

C. Validation test

The three-dimensional flow over a single square cylinder with a spanwise length of $8D$ is chosen to validate the numerical method employed in the present study. The global quantities, such as the mean drag coefficient \bar{C}_D , the root-mean-square (rms) lift coefficient \bar{C}_L , and the Strouhal number St , calculated at three different polynomial orders are provided in Table I. The results reported in the available literature are also presented. The comparison in Table I

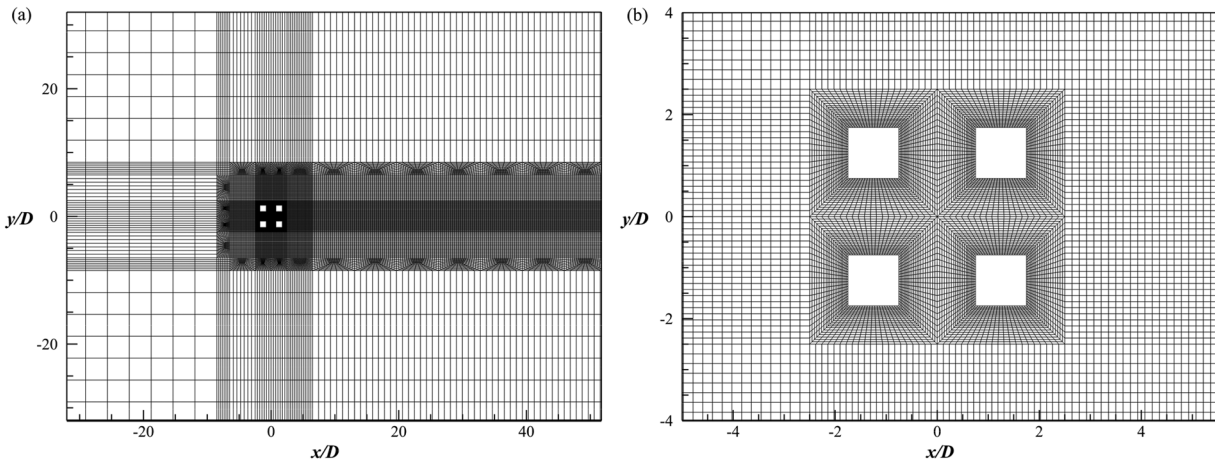


FIG. 2. Grid schematic for $L/D = 2.5$ with $P = 8$ in the x - y plane. (a) Cross-sectional view. (b) Zoom-in view near the four square cylinders in an in-line square arrangement.

TABLE I. Comparisons of the mean drag coefficient, the root-mean-square lift coefficient, and the Strouhal number for a square cylinder at $Re = 150$ and $Re = 300$.

Case	$Re = 150$			$Re = 300$		
	\bar{C}_D	C'_L	St	\bar{C}_D	C'_L	St
Present($P = 6$)	1.463	0.291	0.156	1.488	0.201	0.146
Present($P = 7$)	1.453	0.284	0.156	1.487	0.207	0.146
Present($P = 8$)	1.446	0.282	0.156	1.484	0.202	0.146
Sohankar <i>et al.</i> ³⁵	1.44	0.230	0.165	1.47	0.200	0.153
Doolan ³⁴	1.44	0.296	0.156
Yoon <i>et al.</i> ³⁶	1.43	0.204	0.146

TABLE II. Comparisons of the mean drag coefficient, the root-mean-square drag coefficient, the root-mean-square lift coefficient, and the Strouhal number for SC1 of the four square cylinders with $L/D = 2.5$ at $Re = 200$.

	\bar{C}_D	C'_D	C'_L	St
$P = 6$	1.615	0.0446	0.125	0.132
$P = 7$	1.596	0.0412	0.114	0.132
$P = 8$	1.585	0.0423	0.116	0.132
$P = 9$	1.577	0.0422	0.115	0.132

suggests that the present results are in good agreement with previous studies.^{34–36}

Furthermore, a resolution study for the physical model in question is carried out by varying the polynomial order P . The spatial resolution is controlled by varying the order P of the polynomial, which is interpolated at the Gauss–Lobatto–Legendre quadrature points. For the case of $L/D = 2.5$ and $Re = 200$, the wake development is orderly and regular. The hydrodynamic coefficient is more accurate, which makes the grid accuracy verification more reliable. Therefore, the cases of $L/D = 2.5$ and $Re = 200$ are selected for the grid independence analysis and the results for SC1 with four different polynomial orders ($P = 6, 7, 8$, and 9) are presented in Table II. It can be seen that for order $P \geq 8$, the relative difference is less than 1%, indicating that the solution of meshes with $P \geq 8$ is converged

and can correctly resolve the flow. Considering the computational efficiency, $P = 8$ is used hereafter.

III. RESULTS

In this section, results of the three-dimensional flow over the four-square-cylinder system are presented. It is found that the wake vortex structure presents distinct features at different Re and spacing ratios. The effects of different spacing ratios on wake dynamics and the three-dimensional vortex structures are described in detail for Reynolds numbers of 150 and 200, respectively. For the sake of convenience, each case considered in this section is expressed as “ $L/D - Re$,” such as 1.4–150, 2.5–200, etc.

The laminar to turbulent stage experienced a long transition period, namely, wake transition, shear layer transition, and boundary layer transition, and finally the flow developed into complete turbulence. The three-dimensional unstable mode is generated from the two-dimensional periodic laminar phase to the wake transition phase. In this study, the three-dimensional development of wake is still in the early stage of transition.

Note that the layout of the four square cylinders contains the features of two square cylinders in both side-by-side and tandem arrangements, either of which has its own unique flow topology. When the spacing ratio is small, the structure manifests as a single bluff body, but due to the strong nonlinear effect caused by the gap flow, the three-dimensionality appears to be different from the single square cylinder. As the spacing ratio increases, the interactions between the upper and lower square cylinders are gradually weakened, and the structure can be regarded as a double row arrangement in side-by-side. The vortex streets produced by the upper and lower rows usually appear as symmetrical layout. On account of the sharp corners of the square cylinder, the fluid on the near wall of the bluff body is very different in flow pattern from the surface of the circle cylinder. Hence, in this study, the flow separation of the fluid, the resulting vortex shedding, and the oscillation of the wake vortex have their distinct features.

A. Hydrodynamic forces

The variations of the mean drag coefficient \bar{C}_D and the root-mean-square lift coefficient C'_L at $Re = 150$ are shown in Fig. 3. The results of an isolated square cylinder are also displayed as a comparison. The determination of the two coefficient values is based on at

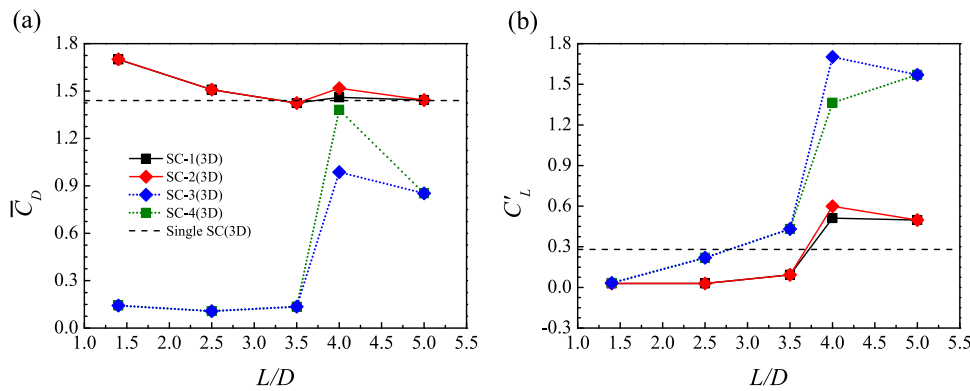


FIG. 3. (a) The line chart of mean drag coefficient at $Re = 150$. (b) The line chart of root-mean-square lift coefficient at $Re = 150$.

least 1000 non-dimensional time when the flow structure is relatively stable. It can be seen that the \bar{C}_D values of the two upstream square cylinders gradually approach the value of the single square cylinder with the increasing spacing ratio. When the spacing ratio increases from 3.5 to 4, the \bar{C}_D values of downstream SC3 and SC4 experience a sudden jump, which is attributed to the fact that the vortices generated from the upstream cylinders are shed in the gap. This phenomenon also leads to the rapid rises of C'_L of the square cylinders at the same L/D , as shown in Fig. 3(b). Note that the values of the force coefficient for the symmetrically arranged upstream SC1 and SC2 are exactly the same, as well as the downstream SC3 and SC4, in the range of spacing ratios considered, with the exception of $L/D = 4.0$. For $L/D = 4.0$, the force coefficient values of the downstream two square cylinders show a larger difference than those of the upstream cylinders. This difference indicates that the wake symmetry may be broken due to the vortex interactions, which will be analyzed later.

Figures 4(a) and 4(b) show the mean drag coefficient \bar{C}_D and the root-mean-square lift coefficient C'_L at $Re = 200$ as a function of L/D , respectively. The three-dimensional numerical results, reported by Lam and Zou²⁰ for the flow over four circular cylinders in an in-line square configuration, are also presented in this figure. The values of \bar{C}_D for the upstream SC1 and SC2 decrease slightly as the spacing ratio increased, while the \bar{C}_D values of the downstream SC3 and SC4 show fluctuations. In general, the values of \bar{C}_D for the square cylinders are larger than their counterparts for the circular cylinders, except that the values of the downstream SC3 and SC4 are lower than those of the circular cylinder at a spacing ratio of $L/D = 2.5$, indicating that the three-dimensionality at this spacing ratio may be quite different from other spacing ratios, which will be presented in the following sections. Note that increasing L/D from 2.5 to 3.5 sees a rapid rise in \bar{C}_D of the downstream square cylinders, due to the vortex shedding in the gap. This means that the occurrence of vortex shedding in the gap is earlier in terms of the spacing ratio, compared with that at $Re = 150$.

For the root-mean-square lift coefficient C'_L shown in Fig. 4(b), C'_L for each square cylinder increases with increasing spacing ratio until $L/D = 4.0$. A significant increase of C'_L from $L/D = 2.5$ to 3.5 is also observed, which is consistent with that of \bar{C}_D presented in Fig. 4(a). For $L/D > 4.0$, the values of C'_L remain almost constant for

the upstream square cylinders, while the values of C'_L decrease for the downstream square cylinders. Even though the geometrical configuration is symmetrically arranged, there still exist some deviations between the upstream cylinders or the downstream cylinders, such as C'_L for SC3 and SC4 at $L/D = 3.5$, due to vortex interactions or the competitions of multiple three-dimensional instabilities, which will be elaborated later.

B. Unstable modal evolution analysis at $Re = 150$

In the three-dimensional direct numerical simulations, 32 Fourier modes are employed to capture the flow variations in the spanwise direction. Calculations with 64 Fourier modes show variations of less than 1% in the hydrodynamic forces and no changes in the observed wake structures, indicating that 32 Fourier modes are enough to accurately capture the small-scale structures in the wake of the configurations considered in the present study. For all the three-dimensional simulations, a low-level white noise of amplitude $10^{-5} U_\infty$ is added to the spanwise velocity component at startup to accelerate the development of the three-dimensional instabilities.

In order to quantitatively investigate the evolution of three-dimensional flow, as well as modal interactions in the wake, the kinetic energy is recorded over time, which is defined as follows:

$$E_k(t) = \frac{1}{2} \int_V \mathbf{u}_k^2 dV, \quad (7)$$

where k is the spanwise wavenumber and V is the volume of the computational domain. One positive and negative solid blue and red iso-surface in the vortex is defined as one periodic vortex pair, corresponding to one wavenumber. As the flow evolves, the unstable wavenumbers will experience an exponential growth stage to gain dominant energies, while the stable wavenumbers will decay. The case of 3.5–150 is chosen to illustrate how the kinetic energy is utilized to analyze the modal evolutions and interactions, as shown in Fig. 5.

It can be seen in Fig. 5 that the energy of each non-zero spanwise wavenumber initially drops rapidly, and then the unstable wavenumbers are observed to grow exponentially in the linear regime ($t \leq 400$). The exponential growth is eventually

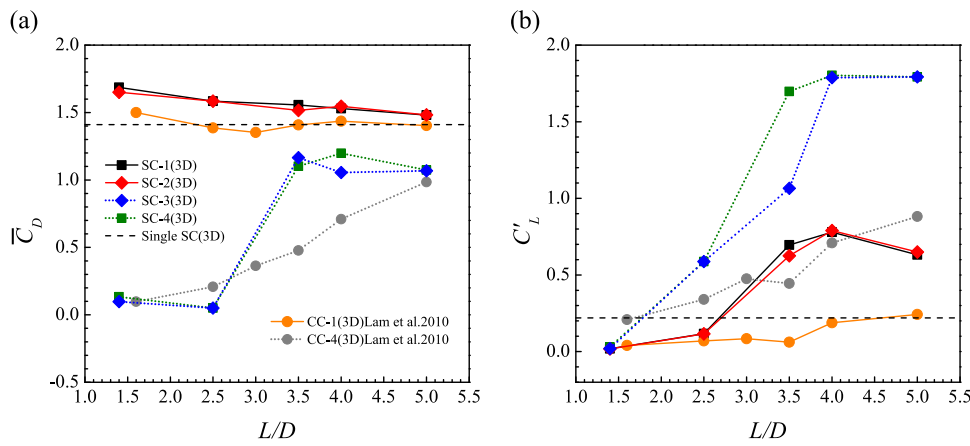


FIG. 4. (a) The line chart of mean drag coefficient comparing with earlier studies for four circular cylinders (marked as CC) at $Re = 200$. (b) The line chart of root-mean-square lift coefficient comparing with earlier studies for four circular cylinders at $Re = 200$.

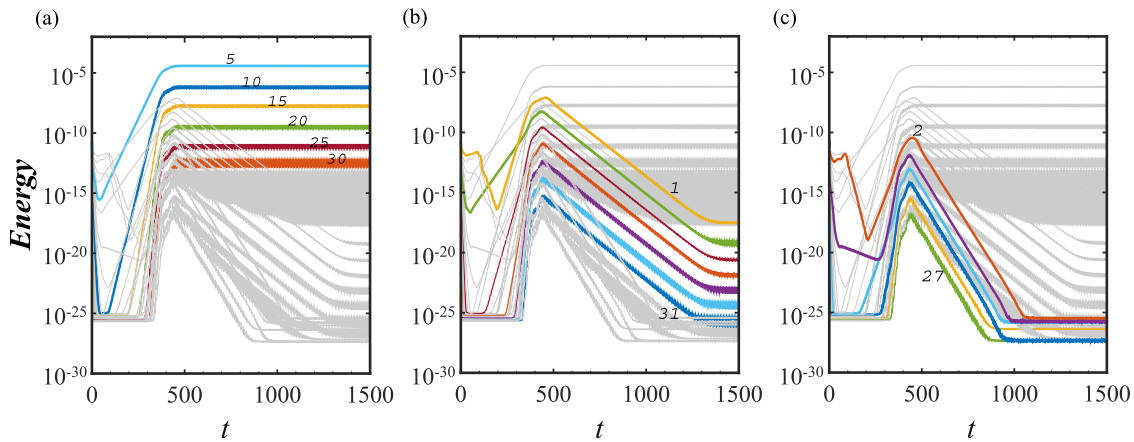


FIG. 5. Energy curves time series of spanwise wavenumbers for $Re = 150$ with a spacing of 3.5. (a) The bold and colored lines express energies of the dominant wavenumber 5 and its harmonics. (b) expresses energies of the dominant wavenumber 1 and its harmonics. (c) expresses energies of the dominant wavenumber 2 and its harmonics.

counter-balanced by the non-linear effects, rendering the flow saturated with a dominant spanwise wavenumber of $K = 5$. Note that the energy in the wavenumber of $K = 5$ is steadily periodic after saturation, indicating that the three-dimensional structure has stopped its further deformation. The harmonics of the dominant wavenumber ($K = 10, 15, 20, 25$, and 30) with much lower energies are also displayed in Fig. 5(a). Energies in the non-harmonic wavenumbers are observed to decay at different rates, part of which can be classified into two groups ($k = 2, 7, 12, 17, 22$, and 27 and $k = 1, 6, 11, 16, 21$, and 26). The wavenumbers within each group share similar energy oscillations over time, and the wavenumber interval in each group is the dominant wavenumber of the highest energy, as can be seen in Figs. 5(b) and 5(c), respectively.

In this study, the time evolutions of energies in the dominant spanwise wavenumbers are mainly focused, as well as the corresponding wake structures, to identify the fundamental mode and illustrate the wake transition process. Transition refers to the mutual conversion between three-dimensional unstable modes in the early stage of wake development.

1. $L/D = 1.4$

In the case of 1.4–150, the energy time series of wavenumbers is shown in Fig. 6(a). After a period of development, the interference of nonlinear effects is more prominent. The main form of expression is the interaction and merging between the vortices, which will promote the occurrence of smaller wavenumber structures. At the same time, small wavenumber Fourier modes compete with each other to obtain energy in the course of a long time.

The trend at the beginning of the energy also shows a rapid decline and then rise in an exponential rate, with the energy value peaking at around $t = 200$. It is worth noting that before vortex-shedding the three-dimensional effect begins to generate [Fig. 6(b)]. As the vortex shedding, the tongue-like vortex gradually transforms into rib-like vortex. The physical mechanism of the transition to three-dimensionality in this stage is revealed and explained by Agbaglah and Mavriplis.³⁷

Subsequently, the curves of all the wavenumbers begin to decrease until about $t = 500$. During this phase, the

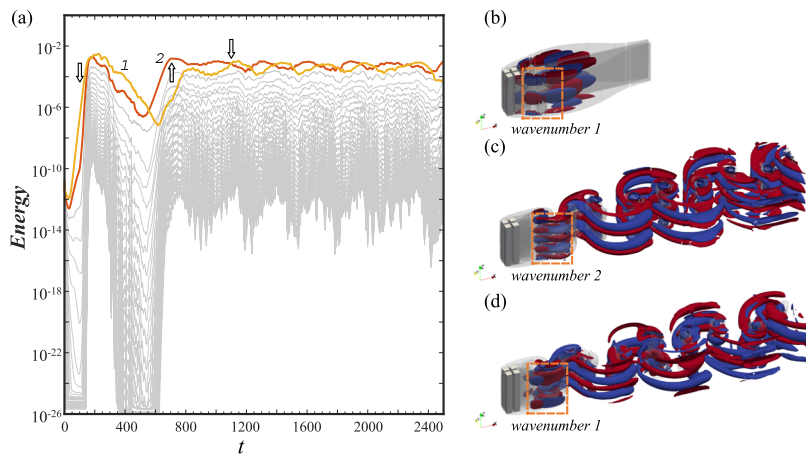


FIG. 6. Time series of main model energies and the instantaneous vorticity for the case of 1.4–150. Solid blue and red surfaces are iso-surfaces of positive and negative streamwise vorticity ω_x and translucent surfaces are iso-surfaces of ω_z . (a) Evolution of wavenumber 1 and 2 is shown in bold and colored lines. (b) Vortex structure at $t = 100$. (c) Vortex structure at $t = 700$. (d) Vortex structure at $t = 1100$.

three-dimensional effect captured by DNS is continuously weakened. In fact, the flow state is still in the laminar state and three-dimensional instability has not yet occurred at low Reynolds numbers. Similar to the majority of previous studies,^{15,38,39} the three-dimensional instability of a single square cylinder fails to appear before $Re = 165$, so this trend is reasonable. What is abnormal is that all wavenumber modes obtain energy again after $t = 500$, and several wavenumbers with higher initial values of energy quickly take the lead. At about $t = 700$, the modal energy with wavenumber 2 is saturated, and then it can be seen that the two modes of wavenumber 1 and wavenumber 2 are constantly competing with each other. The visualized three-dimensional vortex structures at two specific moments are shown in Figs. 6(c) and 6(d). The spanwise vortex tubes show distortion at the time instant $t = 700$. The deformation of the vortex street is caused by the appearance of distortion on the spanwise vortices, which illustrates the generation of three-dimensional instability. At the same time, the streamwise vortex pairs with opposite signs are produced in an alternating form along the spanwise direction. Initially generating three-dimensional instability, the streamwise vortex pairs present an ordered parallel symmetry along the vortex tubes. As shown in Fig. 6(c), the spanwise wavelength of the vortex pairs is approximately 4D, corresponding to wavenumber 2. Then, the vortex structure in the spanwise direction is further deformed, performing irregular characteristics in the flow field. At $t = 1100$ [Fig. 6(d)], the spanwise wavelength in the wake vortex structure is still 4D, but it appears as one periodic vortex

pair in the near-wake region, which is in the modal mutual interference stage [Fig. 6(a)]. Up to $t = 2500$, streamwise vortices return to the regular parallel vortex pairs of two cycles, which is almost identical to that in Fig. 6(c). In general, the spanwise wavelength is dominant in 4D in the evolution of the wake vortices with $L/D = 1.4$, which is similar to the form of mode A in a single square cylinder. The characteristics of the evolution of three-dimensional flow vortex structure over time are illustrated quantitatively by the energies.

From the vorticity contours, the flow structure appears as a single bluff body wake pattern. What is outstanding is that the impact of the gap flow is clearly shown in Fig. 7(a). The time history curve of force components shows a legible pulsation as well as the apparent intermittent switching of the flow pattern in Figs. 7(b) and 7(c). Carini *et al.*⁴⁰ have found the origin of the intermittent switching of the flow pattern at low Reynolds number. On the basis of the energy curves, the dominant wavenumber 2 mode is in line with the high frequency, and the interference of the low frequency corresponding to other modes weakens the ordered flow vortex structure of the wavenumber 2 mode. Modal competition has been in a cyclical progression.

Sau *et al.*⁴¹ have investigated that the vortex structure gradually loses stability and induced three-dimensionality as the spacing ratio decreases, and corelines of the shedding vortex appear in a wave-like shape. It is noted that in the range of 0.2–1 spacing ratio the gap flow is randomly flipped between the two cylinders

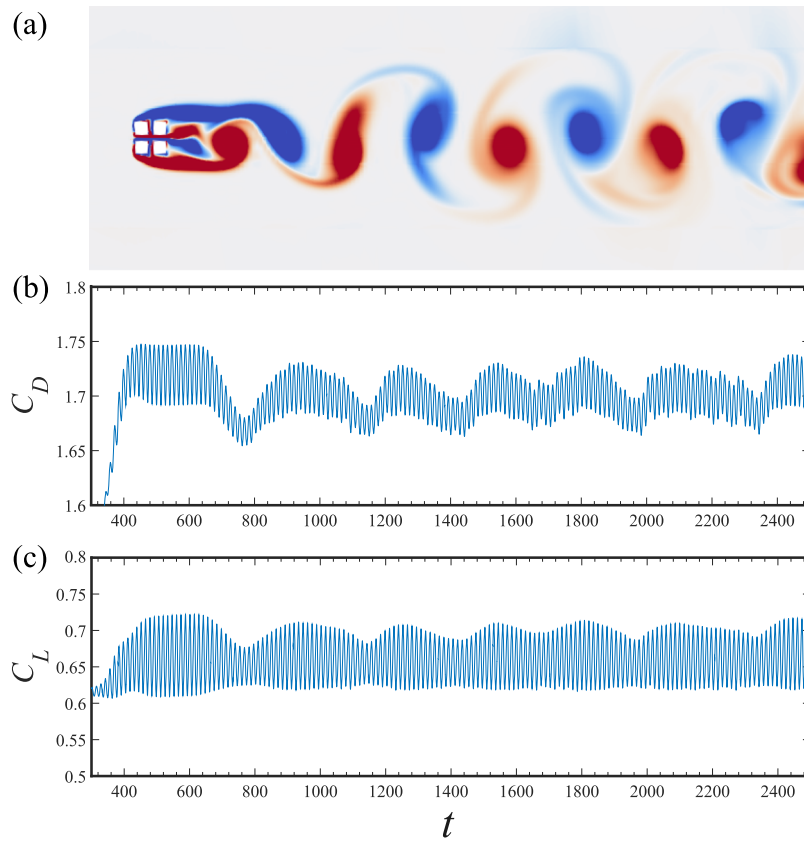


FIG. 7. The case of 1.4–150. (a) The middle section of instantaneous spanwise vorticity contours. (b) Time history curves of drag coefficient. (c) Time history curves of lift coefficient.

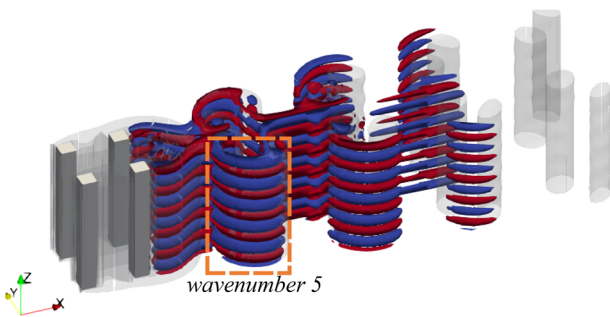


FIG. 8. For the case of 3.5–150, solid blue and red surfaces are iso-surfaces of positive and negative streamwise vorticity ω_x and translucent surfaces are iso-surfaces of ω_z . The vortex structure at $t = 1500$.

and alternately deflected towards one cylinder or the other, and the spanwise extending vortex tube begins to generate a wave characteristic. The above energy phenomenon and the corresponding three-dimensional vortex structure transformation can be understood as the effect of the gap flow on the generation of the three-dimensional wake of the structure with a small spacing at a low Reynolds number.

2. $L/D = 3.5$

As shown in Fig. 5(a), the energy curves show that wavenumber 5 reaches saturation and occupies the global dominant mode, meanwhile its harmonics array tends to plateau with time, nevertheless the energy values of the other group arrays are declining.

Since the energy value of wavenumber 10 is low, it is not reflected in the three-dimensional flow vortex structure. The extremely ordered spanwise vortices of waviness and rib-shaped streamwise vortices are shown in Fig. 8. There are five cycles of vortex pairs along the spanwise direction, corresponding to the wavelength of about 1.6D, which perfectly corresponds to the dominant wavenumber in energy curves. Given that a symmetric arrangement of multiple bluff bodies of a certain Reynolds number and a certain range of spacing ratios may be critical to the stable development of the wake vortex structure, these ordered vortex structures in a certain spacing may serve as key points in the future study of the flow transition process. In addition, the spanwise wavelength exhibits the features of mode C type for 3.5–150.

In the case of 3.5–150, the flow regime appears as a reattachment anti-phase wake pattern from the vorticity contours. It is worth noting that during the process of vortex shedding, the reason of vortex streets on the upper and lower sides spreading outwards is not explicit. After the flow field is fully developed, the amplitude and frequencies in time history curves are kept constant over time, reflecting that the flow field has remained stable.

3. $L/D = 4$

At a spacing ratio of 4, the wake field is a phase-difference pattern. It can be seen from Fig. 10 that the inner vortex of the upper and lower vortex streets starts merging and a new wake flow pattern remains constant after $t = 1600$. In general, the corresponding energy curves without the three-dimensional effect will decay faster. What is unusual is that the energies do not decay thoroughly for the case of 4–150, and after turning point around $t = 1600$

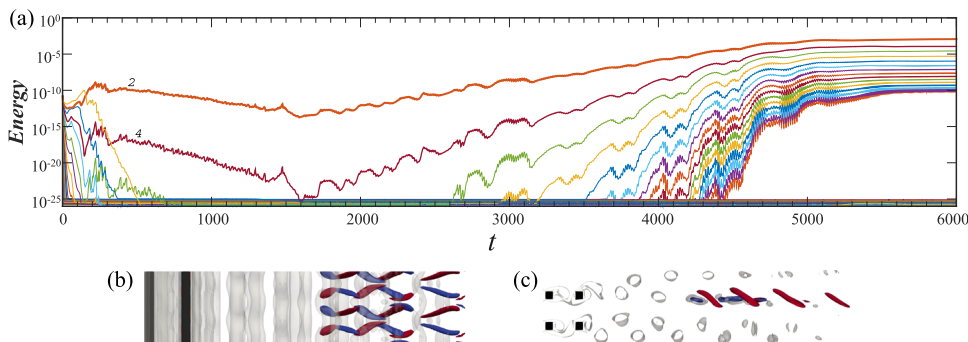


FIG. 9. (a) Evolution of energy curves over time for the case of 4–150. The main wavenumbers 2 and 4 are shown by orange and red lines. (b) The front view of vortex structure at $t = 6000$. (c) The top view of vortex structure at $t = 6000$.

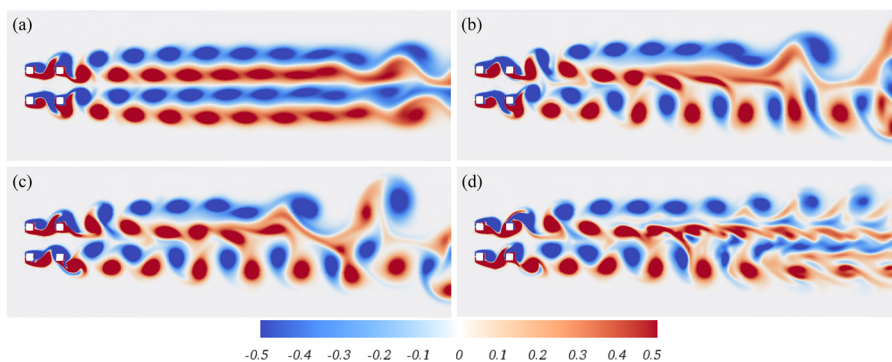


FIG. 10. Evolution of wake flow topology over time with a spacing ratio of 4 at $Re = 150$. (a) $t = 1000$. (b) $t = 1600$. (c) $t = 3000$. (d) $t = 6000$.

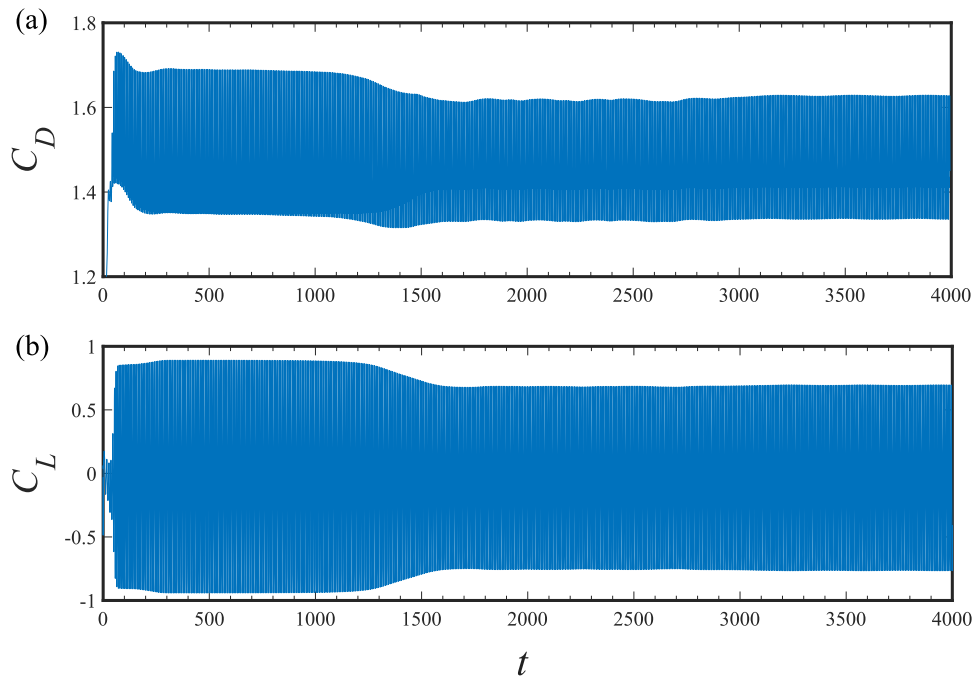


FIG. 11. The case of 4–150. (a) Time history curves of drag coefficient. (b) Time history curves of lift coefficient.

the curves begin to rise. As can be seen from Fig. 9, the ascending process keeps very slow, and the emergence and growth of three-dimensional effects are also slow. The evolution of the energies continues to be tracked. After $t = 5500$, all harmonics reach plateau and wavenumber 2 dominates. The fusion process of the inner vortex in the far-wake is shown in Figs. 10(a)–10(c), and it is seen in Fig. 10(d) that the wake eventually stabilizes. From time history curves (Fig. 11), the trend of wake transition can also be reflected.

Due to the insufficient length of the downstream flow field, a completely stable flow regime in far-wake was not demonstrated. This merging mechanism of the wake vortex illustrates why three-dimensional instability occurs at high spacing and low Reynolds numbers.

4. Two-dimensional laminar flow

There is no three-dimensional effect in the wake flow of the four square cylinders with 2.5–150 and 5–150. The energy curves rapidly decline to the bottom. Despite this, the two-dimensional wake flow pattern of each spacing ratio has its own features. The details and features of the wake flow will be explained later.

Unlike the spacing of 1.4 and 3.5, no three-dimensional instability occurs in the case of 2.5–150. The flow patterns in the near-wake region with spacing ratios from 3.5 to 5 are all in the form of an anti-phase synchronization at $Re = 150$, in which the three-dimensional intensity generated by $L/D = 3.5$ continuously enhances with time. The flow regime of $L/D = 2.5$ is monitored over time in Fig. 12, and the initial phase also performs an anti-phase synchronous pattern. The wake transition starts around $t = 347$, and the saltation of the time history curve at this time in Figs. 13(a) and 13(b)

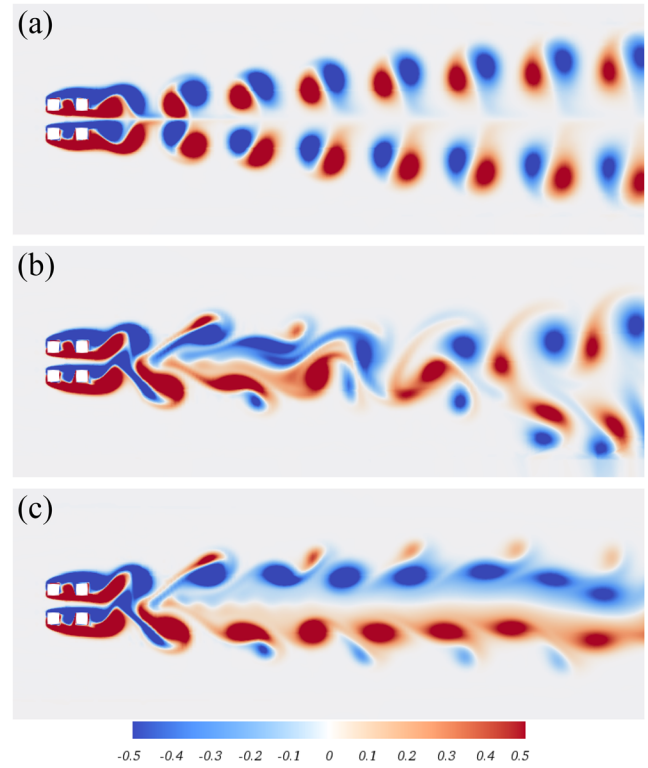


FIG. 12. Evolution of wake flow topology over time with a spacing ratio of 2.5 at $Re = 150$. (a) $t = 200$. (b) $t = 347$. (c) $t = 500$.

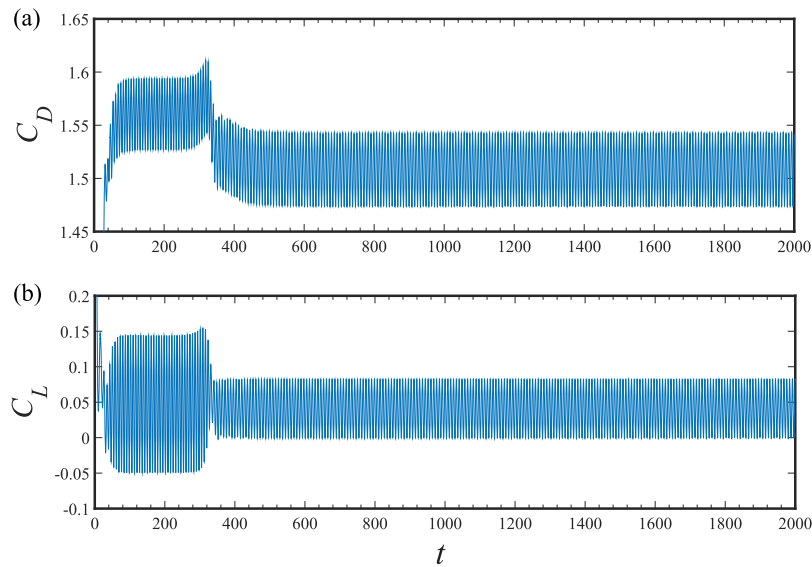


FIG. 13. The case of 2.5–150. (a) Time history curves of drag coefficient. (b) Time history curves of lift coefficient.

indicates the transform. The flow regime switches from anti-phase to in-phase, which does not revert in the later development. The reason why such a change process does not produce a three-dimensional effect at this spacing may be that itself avoids the three-dimensional instability of the spanwise direction by the evolution of mechanism of the flow topology. Increasing in spacing, the flow field cannot be stabilized by changing the flow topology, so the three-dimensional effect begins and further develops.

In addition, for 5–150, the wake flow expresses the upstream vortex shedding anti-phase pattern. The vortex streets on the upper and lower sides themselves change the vortex shedding frequency at the far-wake. This variation does not cause new three-dimensional effects.

C. Unstable modal evolution analysis at $Re = 200$

The results of the existing studies indicate that the wake vortex structure of a square cylinder at $Re = 200$ has completely generated three-dimensional instability and is in the process of mode transition. There is little research on the evolution of vortices of multiple bluff bodies and the following describes the situation when $Re = 200$.

1. $L/D = 1.4$

At $Re = 200$, the generation of three-dimensional instability is no longer caused mainly by the influence of the gap flow. As shown in Fig. 14(a), different from the previous cases, there is no stage in which the trends of the model energy first drops, and then rises.

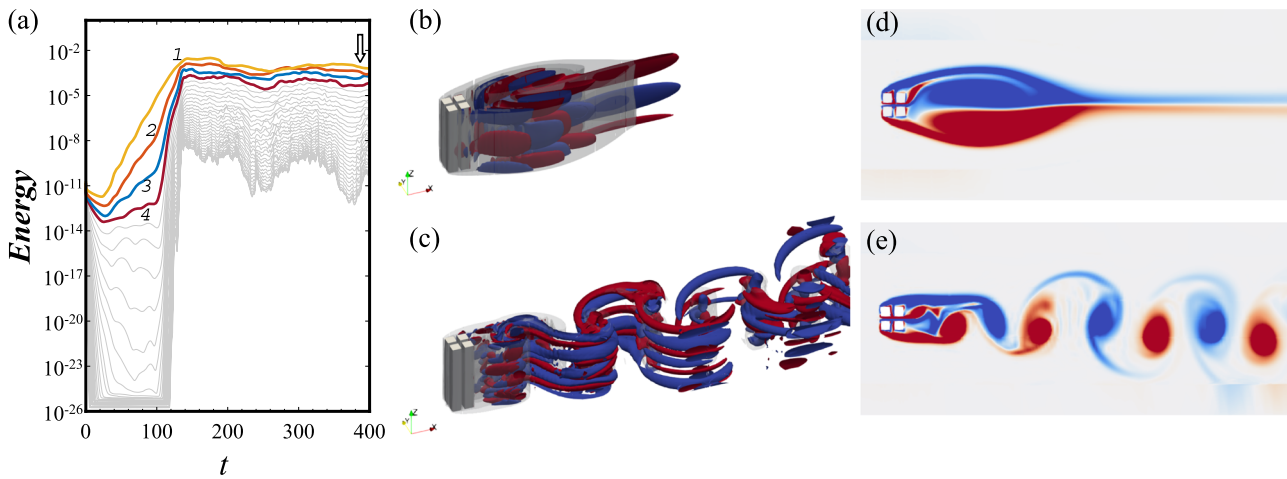


FIG. 14. For the case of 1.4–200. (a) Time series of main model energies, evolution of wavenumber 1 ~ 4 shown in bold and colored lines. [(b) and (c)] The three-dimensional instantaneous vortex structures at $t = 100$ and $t = 400$, respectively. [(d) and (e)] The middle section of instantaneous spanwise vorticity contours at $t = 100$ and $t = 400$, respectively.

At small spacing ratios, the two-dimensional flow state is close to the case of a single square cylinder, but the onset and evolution of three-dimensional instability is under the influence of many factors, where the gap flow plays a pivotal role. The high-intensity gap flow enhances the nonlinear effect, which is manifested by the excitation of the wake field, and causes the small-scale vortex to merge and develop into a larger-scale vortex. In the case of a single square cylinder with $Re = 200$, the three-dimensional instability is in the transition interval, and it mainly appears when mode B is in the evolution of time.

A large amount of wavenumber modes absorb more energy, so it is difficult to quantify its dominant mode as shown in Fig. 14(a). In the early stage of wake evolution, the three-dimensional instability has emerged before vortex-shedding [Figs. 14(b) and 14(d)], which is the same as in the case of 1.4–150. However, when the spacing is greater than 1.4, the vortex has shed before the three-dimensional instability occurs. By observing the three-dimensional flow vortex structure after vortex shedding [Fig. 14(b)], the wake flow presents a single vortex street form. In this study, it can be observed that there are multiple cycles of vortex pairs coexisting, corresponding to the spanwise wavelength in the range from 2D to 4D. It can be seen as a single bluff body structure on account of sufficiently small spacing ratio, so the flow characteristics of the wake vortex can be compared with a single square cylinder. Jiang *et al.*³⁸ investigated the three-dimensional wake transition of a single square cylinder. The transition from mode A* to mode B is in the interval of $Re = 185$ –210, so the coexistence and interaction of mode A with dislocation and mode B can evolve in this range. Meanwhile, there are multiple vortices of different scales dislocated, which is similar to the phenomenon of the single square cylinder reported by Jiang *et al.*³⁸

Comparing the vorticity contours of the two cases of 1.4–150 and 1.4–200 demonstrated in Figs. 7(a) and 14(e), both of which appear as a single bluff-body wake pattern. For the case of 1.4–200, increased strength of the gap flow directly impacts the mature vortices and then disturbs the stability of the shedding vortex, making the features of three-dimensional unstable mode transition not the same as the stage of mode A to mode B.

2. $L/D = 2.5$

When the spacing ratio is 2.5 (Fig. 15), the entire development process of this stage keeps exceedingly regular. The dominant spanwise wavelength of streamwise vortices appears to be 1.6D approximately, corresponding to the five cycles of rib-shaped vortex pairs. It may be seriously noted that both two cases (3.5–150 and 2.5–200) have a completely similar three-dimensional instability mode according to whether three-dimensional numerical simulation or energy curves. The unstable mode of wavenumber 5 has a typical significance and takes the lead in the four square cylinder structure under uniform flow [Fig. 15(a)]. The phenomenon that this type of wake vortex is different from that of single bluff body manifests that multiple bluff body structures have unique hydrodynamic characteristics and mechanism.

Both cases of 3.5–150 and 2.5–200 show a spanwise wavelength of 1.6D. This is similar to the third fundamental mode found in recent studies,^{9–12,42} referred to as mode C, which is characterized by the double-period and intermediate spanwise wavelength. It can

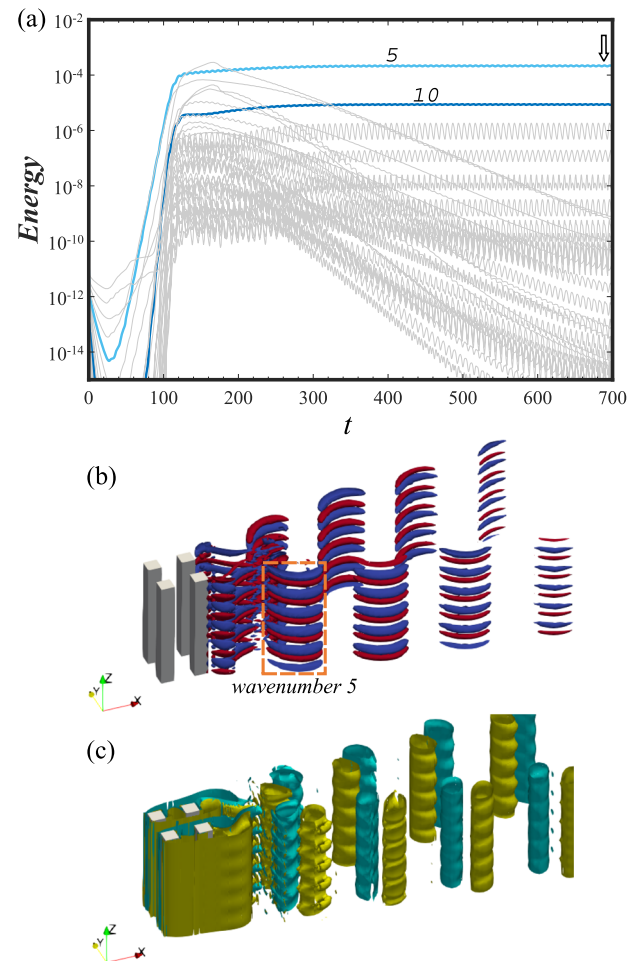


FIG. 15. For the case of 2.5–200. (a) Time series of main model energies, evolution of wavenumber 5 and 10 shown in bold and colored lines. (b) Iso-surfaces of ω_x shown by blue and red surfaces. (c) Iso-surfaces of ω_z shown by light green and dark green, respectively.

be determined from Fig. 16, which indicates the features of double-period in streamwise vortices, that both three-dimensional instabilities are mode C. No matter from the energy curves or the vortex structure, there is no evidence of other instability mode and mode C keeps absolutely dominant. At the same time, the flow regime all appears as a reattachment anti-phase flow pattern shown in spanwise vortices.

3. $L/D = 3.5$

The spacing ratio of 3.5 becomes a key node. At this moment, the flow state enters a chaotic state, which shows that the disturbance between the modes becomes very intense. The three-dimensional instability under this stage is undergoing a new transition process. The initial performance is dominated by wavenumber 2 shown in Fig. 17(a). The spanwise wavelength of streamwise vortices presents approximately 4D. After that, the remaining wavenumber modes

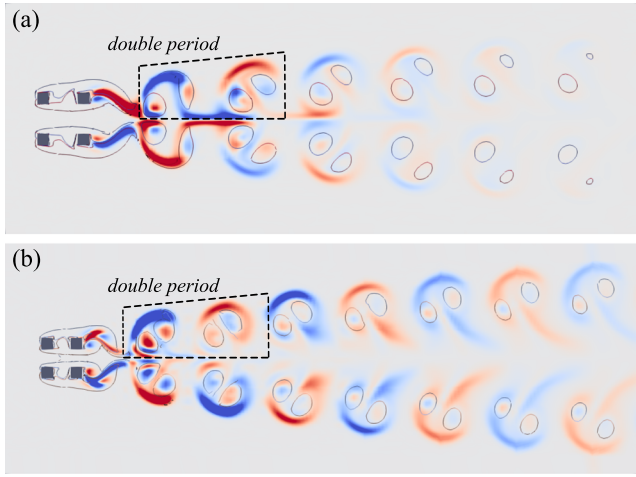


FIG. 16. The features of period-doubling mode shown in instantaneous streamwise vorticity contours. Spanwise vorticity is overlaid as solid lines. (a) 3.5–150. (b) 2.5–200.

rise rapidly and compete fiercely with wavenumber 2, and the energy oscillations reflect the fierceness of nonlinear effects. Noteworthy it may be that the uniformity and regularity of the wake flow field begin to degenerate, and more broken and dispersed vortices surround the dominant vortex pairs. Two time points of $t = 1500$ and $t = 2000$ are selected and shown in Figs. 17(c) and 17(d). At the previous time, modes of wavenumbers 2 and 3 are basically not dominant, and the vortex structure shows incline and interlacing. Whereafter, the mode of wavenumber 3 is slightly dominant, and the three-period flow vortices in the vortex structure are relatively neat and parallel to the flow direction. Throughout the evolution process, the three-dimensional flow vortices are in chaotic states.

In addition to wavenumbers 2 and 3 as the leading mode, wavenumber 1 occupies a higher energy. In the example of multimodal competition in this article, it has appeared many times. For this phenomenon, it does not mean that wavenumber 1 dominates, because it cannot be reflected from the wake vortex structure. Mainly, the energy curves have a good quantitative orientation for the relatively regular single wavenumber mode. It is difficult to capture the multimodal chaotic state, so the flow field along the span is recognized as one period.

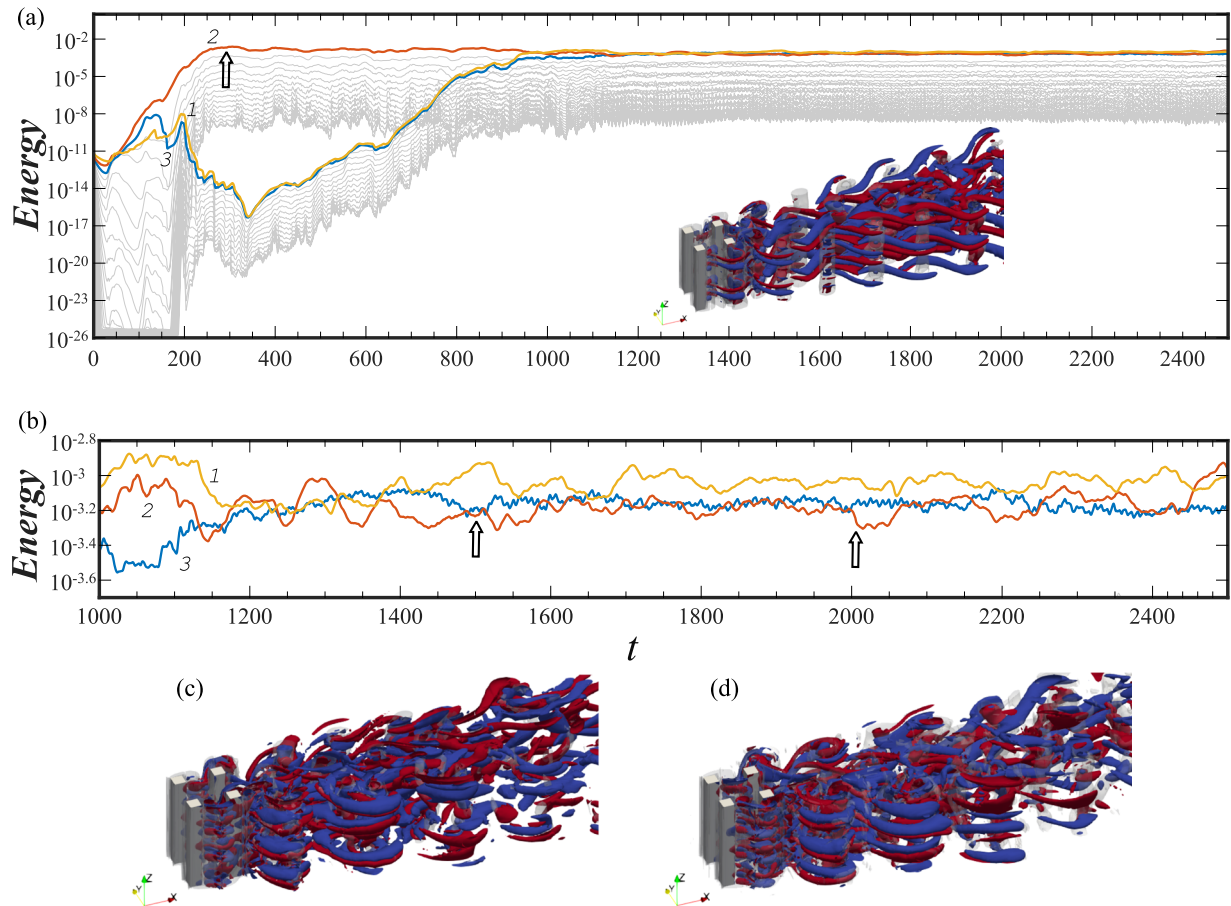


FIG. 17. Time series of main model energies and the instantaneous vorticity for the case of 3.5–200. (a) Evolution of wavenumbers of 1, 2, and 3 shown by bold and colored lines. Vortex structure at $t = 300$. (b) Partially enlarged view of (a) of the energy curves ranging from $t = 1000$ to $t = 2500$. (c) Vortex structure at $t = 1500$ on the left. (d) Vortex structure at $t = 2000$ on the right.

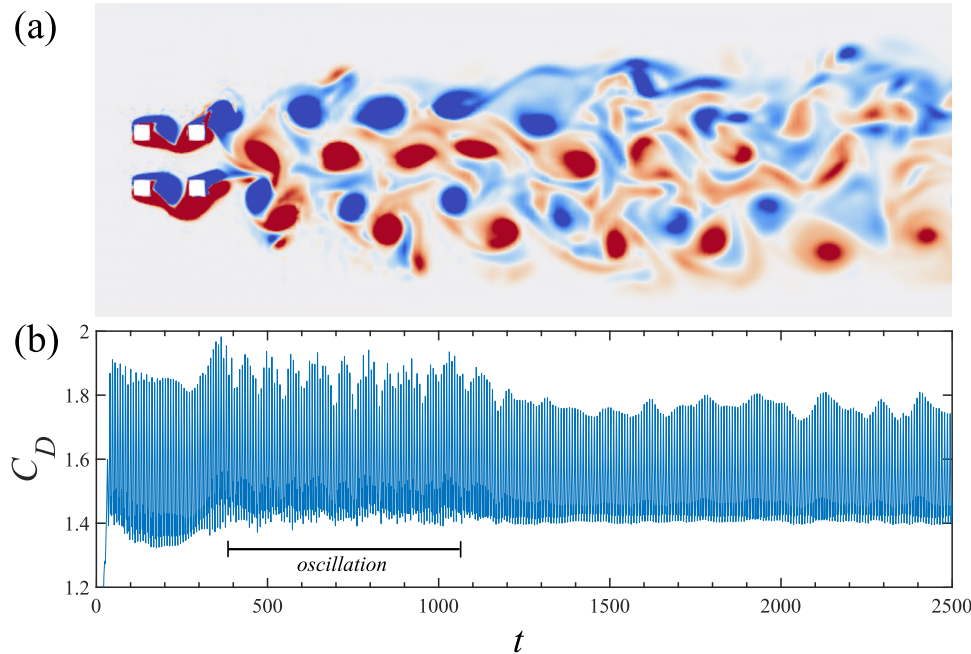


FIG. 18. The case of 3.5–200. (a) The middle section of instantaneous spanwise vorticity contours. (b) Time history curves of drag coefficient.

The wake pattern looks very turbulent, as shown in Fig. 18(a). The wake of the rear of upstream square cylinders put up the state of the in-phase and at the critical point of vortex shedding. The reason why the three-dimensional instability appears exceedingly intense is that they are in the stage of multi-modal mutual interference. As shown in Fig. 18(b), the amplitude and frequency oscillations of the time history curve are severe in the first $t = 1000$, in which wavenumber 2 dominates and the fluctuation of force of square cylinder 1 is obvious. After the stage of intense interactions of two modal, the amplitude of the drag and lift curve is relatively stable, which highlights that the modal mutual interference is the dominant state under this condition. Since the vorticity contour is a section of three-dimensional vortex, major broken vortex structures are prominent. By observing the main vortex core, the downstream wake illustrates

a form of phase difference and the vortex shedding frequency is also different.

4. $L/D = 4$

Passing the previous chaotic state, the flow state enters a new stable regime again. After a period of development, the energies reach saturation and become the dominant mode with wavenumber 2, which lasts for about $t = 900$ as shown in Fig. 19. The energy branches out two groups of wavenumbers during this time and the other groups lose energy and begin to decline.

The development of the three-dimensional flow structure launches out into transition at 900 time unit. The mode group where the main wavenumber 2 and its corresponding harmonic are located

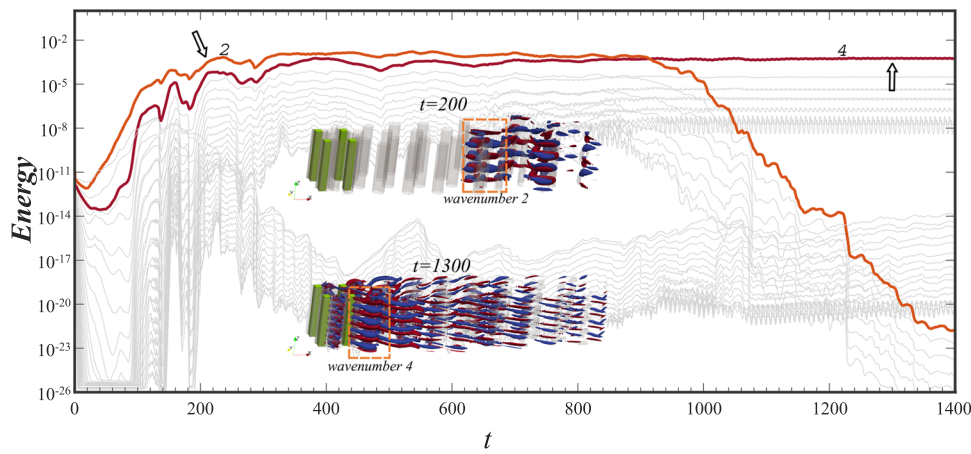


FIG. 19. Energy curves time series and two instantaneous vorticities in different stages for the case of 4–200. The dominant wavenumbers 2 and 4 are shown by bold and colored lines. The upper and lower figures represent the vortex structures at $t = 200$ and $t = 1300$, respectively.

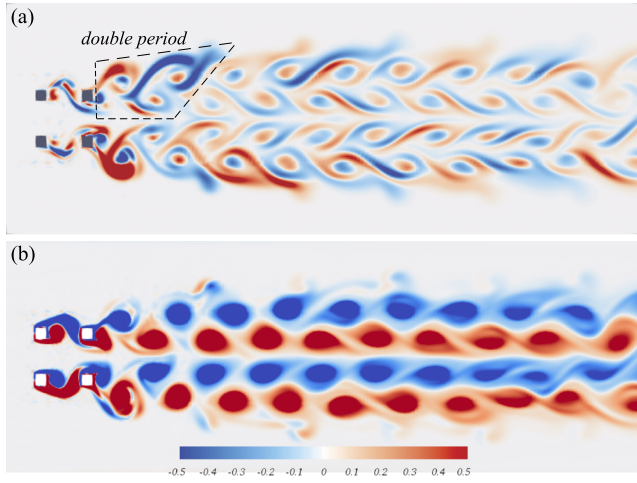


FIG. 20. The case of 4–200, $t = 1300$. (a) The features of period-doubling mode shown in instantaneous streamwise vorticity contours. (b) The features of instantaneous spanwise vorticity contours.

comes into bifurcation and the branches are divided into two new groups. Wavenumber 2 is replaced by wavenumber 4 to turn into the dominant mode, while wavenumber 2 as well as its harmonic decay rapidly. A four-period spanwise vortex pair emerges a regular modality, corresponding spanwise wavelength of 2D.

It can be seen from the comparison of two three-dimensional flow structures that the initial spanwise wavelength of 4D is only a transitional flow state, and the three-dimensional effect is first generated at the far-wake. To a great extent, the instability seems to be due to the coactions of the downstream vortices. Thus, it takes the lead in obtaining energy to generate three-dimensional instability. Along with the vortex at the far-wake flows into a steady state, the energies of the entire flow field are redistributed. In the rear of the square cylinders, the intrinsic spanwise vortices are formed.

As shown in Fig. 20, the latter stage instability is also expressed as mode C, but its spanwise wavelength corresponding to wavenumber 4 dominated is slightly larger than the previous case. The studies of wake transition in staggered cylinders by Carmo *et al.*¹² have shown that mode A and mode B first stemmed in the near-wake of the upstream cylinder, while mode C originated in the near-wake of the downstream cylinder. However, the vortex instability of mode C is generated behind the upstream square cylinder at a spacing of

4. The reason for this phenomenon may be the result of a combination of large bluff body spacing and geometrical shape. A sufficiently large spacing causes the upstream vortex shedding, and this appearance is likely to the downstream mode C instability reacting to the upstream rear vortex, which is synchronously developed into mode C.

5. $L/D = 5$

When the spacing ratio increases to 5, the mutual influence between the square cylinders is relatively weak and its characteristics can be compared with a single square. The wake characteristics of two side-by-side square cylinders at a high spacing ratio are closer to the single square except for in-phase and anti-phase flow pattern. Due to the special arrangement of the four square cylinders, the shedding vortex generated from the upstream square cylinders will flap on the downstream square cylinders, thereby changing the overall flow topology at the far-wake. Nevertheless, a sufficiently large spacing ratio is capable of generating a complete period of shedding vortex behind the upstream cylinders, which is not subject to downstream interference. As shown in Fig. 21, the flow vortex pairs generated after the upstream square cylinders show seven cycles corresponding to the spanwise wavelength of about 1.1D. Compared with the single square cylinder, the three-dimensional instability remains as resemble as mode B. However, the perturbation of spanwise wavelength manifests in the far wake. Among them, the vortex pairs behind the downstream square cylinders also appear in different scales. On account of the nonlinear effects, the interaction of the vortices gives rise to the emergence of small-scale vortex into a large-scale streamwise vortex and further starts oscillation.

By comparison, the values corresponding to each wavenumber reaching saturation keep high, indicating that the final state of the three-dimensional structure is affected by many different unstable modes and suggesting that the transition is a chaotic flow.

Many studies have shown that a symmetric multi-bluff body promotes the most stable pattern to be an anti-phase flow regime. Comparing the two vorticity contours of the case of 4–200 [Fig. 20(b)] and 5–200 (Fig. 22), the flow topology of the wake field in the near-wake is almost identical. However, the two vortex streets develop independently for the case of 5–200, whose disturbance starts at the far-wake shown in Fig. 22, but the impacts on the rear of the upstream square cylinder and the near-wake are consistent with the results of earlier investigations. The four square cylinders at a high spacing ratio are close to a single square, which is in the transition stage at $Re = 200$.

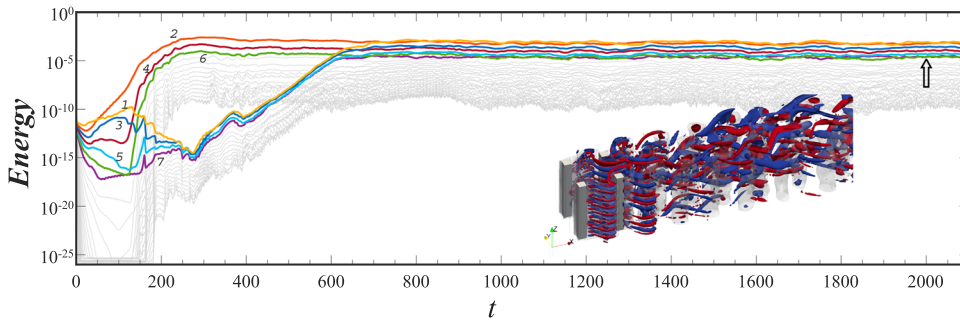


FIG. 21. Energy curves time series and the instantaneous vorticity at $t = 2000$ for the case of 5–200. Wavenumbers 1–7 are shown by bold and colored lines.

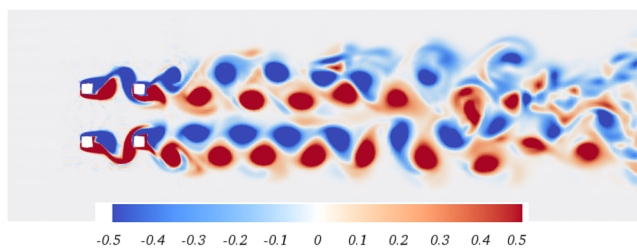


FIG. 22. The features of instantaneous spanwise vorticity contours for 5–200 at $t = 2000$.

IV. CONCLUSION

In this paper, the high-order spectral element method is employed to analyze the development of three-dimensional instability for the four square cylinders. Reynolds numbers of 150 and 200 are selected, and five spacing ratios are adopted, including 1.4, 2.5, 3.5, 4, and 5. The influence of L/D on force characteristics implies that there are specific three-dimensional unstable mode transition processes under four square cylinder conditions. These processes are analyzed qualitatively through three-dimensional visualization vortex structures and are quantified by energy curves. Then, the wake patterns and time-history curves are used to further explain the cause and mechanism of the process of three-dimensional unstable mode transition.

A variety of modal transition processes has emerged by varying the Reynolds number and spacing ratio, which are the major factors affecting the evolution of three-dimensional instability, as well as the flow topology.

The fundamental instabilities of mode A and mode B have appeared for the two end spacings of 1.4 and 5 in this study, which is consistent with earlier correlational studies. However, between the above, the diversity of the three-dimensional vortex structure and the transition of flow topology take on their own characteristics. It was found that at a low Reynolds number of $Re = 150$, at which the wake of a single square cylinder is two-dimensional, the three-dimensional transition phenomenon occurred in flow past four square cylinders.

At low Reynolds number and low spacing, three-dimensional effects appear due to the excitation of the gap flow, and mode A dominates. In the case of 2.5–200 and 3.5–150, an ordered three-dimensional instability mode C with the corresponding spanning wavelength of 1.6D becomes the dominant mode. Meanwhile, for the case of 4–200, the first three-dimensional unstable mode is replaced by the ordered mode C after the end of the disturbance of the far-wake flow in the early stage, and the corresponding spanwise wavelength keeps 2D, slightly larger than the previous 1.6D. The discrepancy of mode C at $L/D = 4$ is that the generated position appears in the rear of upstream square instead of the downstream square. For the case of 3.5–200, between 2.5 and 4, a chaotic regime with severe disturbances appears, indicating that this spacing is in the critical position of multi-modal competition. In this study, the three-dimensional instability mode C was found for the first time in symmetrically arranged multi-column structure. In previous studies, mode C was usually only generated in the wake of the asymmetrical structure.

The flow topology structures can be divided into several main wake patterns via the plane vorticity contours, including a single bluff body pattern, reattachment anti-phase pattern, reattachment in-phase pattern, phase difference pattern, and vortex shedding anti-phase pattern, which reflect the relevant characteristics of the evolution of three-dimensional instability. The flow patterns corresponding to mode C in this study are all in anti-phase synchronization. The evolution of the vorticity contours with $Re = 150$ further reveals the causes of the three-dimensional effect at low Reynolds numbers. For the case of 2.5–150, the generation of three-dimensional instability is avoided by changing its own flow topology. For the case of 4–150, on account of the mechanism of the inner vortex fusion at the far-wake with a long period of development, the three-dimensional effects appear at a low Reynolds number and high spacing ratio for the first time.

ACKNOWLEDGMENTS

The financial support from the National Natural Science Foundation of China (Grant Nos. 51879160, 51809170, 11772193, and 51679139), National Natural Science Funds for Distinguished Young Scholars (Grant No. 51825903), Joint Funds of the National Natural Science Foundation of China (Grant No. U19B2013), Shanghai Natural Science Foundation (Grant Nos. 17ZR1415100 and 18ZR1418000), and Project of Thousand Youth Talents is gratefully acknowledged. This research is also sponsored in part by the Program for Professor of Special Appointment (Eastern Scholar) at Shanghai Institutions of Higher Learning (Grant Nos. ZXDF010037 and ZXDF010040), Program for Intergovernmental International Cooperation Projects of Shanghai Municipality (Grant No. 18290710600), Innovation Program of Shanghai Municipal Education Commission (Grant No. 2019-01-07-00-02-E00066), Program for International Cooperation of Shanghai Science and Technology (Grant No. 18160744000), and State Key Laboratory of Ocean Engineering (Grant No. GKZD010075).

NOMENCLATURE

ω_x	the streamwise vorticity
ω_z	the spanwise vorticity
\bar{C}_D	the mean drag coefficient
C_D	the drag coefficient
C'_D	the root-mean-square drag coefficient
C_L	the lift coefficient
C'_L	the root-mean-square lift coefficient
D	the side length of the square
L	the center-to-center spacing
L/D	the spacing ratio
Re	the Reynolds number
St	the Strouhal number

REFERENCES

- ¹C. H. K. Williamson, "Vortex dynamics in the cylinder wake," *Annu. Rev. Fluid Mech.* **28**(1), 477–539 (1996).
- ²C. H. K. Williamson, "Three-dimensional wake transition," *J. Fluid Mech.* **328**, 345–407 (1996).
- ³D. Barkley and R. D. Henderson, "Three-dimensional floquet stability analysis of the wake of a circular cylinder," *J. Fluid Mech.* **322**, 215–241 (1996).

- ⁴R. D. Henderson, "Nonlinear dynamics and pattern formation in turbulent wake transition," *J. Fluid Mech.* **352**, 65–112 (1997).
- ⁵C. H. K. Williamson, "The existence of two stages in the transition to three-dimensionality of a cylinder wake," *Phys. Fluids* **31**(11), 3165–3168 (1988).
- ⁶J. Robichaux, S. Balachandar, and S. P. Vanka, "Three-dimensional floquet instability of the wake of square cylinder," *Phys. Fluids* **11**(3), 560–578 (1999).
- ⁷H. M. Blackburn and J. M. Lopez, "On three-dimensional quasiperiodic floquet instabilities of two-dimensional bluff body wakes," *Phys. Fluids* **15**(8), L57–L60 (2003).
- ⁸H.-Q. Zhang, U. Fey, B. R. Noack, M. König, and H. Eckelmann, "On the transition of the cylinder wake," *Phys. Fluids* **7**(4), 779–794 (1995).
- ⁹G. J. Sheard, M. C. Thompson, and K. Hourigan, "From spheres to circular cylinders: The stability and flow structures of bluff ring wakes," *J. Fluid Mech.* **492**, 147–180 (2003).
- ¹⁰G. J. Sheard, M. J. Fitzgerald, and K. Ryan, "Cylinders with square cross-section: Wake instabilities with incidence angle variation," *J. Fluid Mech.* **630**, 43–69 (2009).
- ¹¹G. J. Sheard, M. C. Thompson, and K. Hourigan, "Subharmonic mechanism of the mode c instability," *Phys. Fluids* **17**(11), 111702 (2005).
- ¹²B. S. Carmo, S. J. Sherwin, P. W. Bearman, and R. H. J. Willden, "Wake transition in the flow around two circular cylinders in staggered arrangements," *J. Fluid Mech.* **597**, 1–29 (2008).
- ¹³B. S. Carmo, J. R. Meneghini, and S. J. Sherwin, "Secondary instabilities in the flow around two circular cylinders in tandem," *J. Fluid Mech.* **644**, 395–431 (2010).
- ¹⁴C.-B. Choi and K.-S. Yang, "Three-dimensional instability in the flow past two side-by-side square cylinders," *Phys. Fluids* **25**(7), 074107 (2013).
- ¹⁵C.-B. Choi, Y.-J. Jang, and K.-S. Yang, "Secondary instability in the near-wake past two tandem square cylinders," *Phys. Fluids* **24**(2), 024102 (2012).
- ¹⁶K. Lam, J. Y. Li, K. T. Chan, and R. M. C. So, "Flow pattern and velocity field distribution of cross-flow around four cylinders in a square configuration at a low Reynolds number," *J. Fluids Struct.* **17**(5), 665–679 (2003).
- ¹⁷K. Lam, J. Y. Li, and R. M. C. So, "Force coefficients and Strouhal numbers of four cylinders in cross flow," *J. Fluids Struct.* **18**(3–4), 305–324 (2003).
- ¹⁸K. Lama and L. Zou, "Experimental and numerical study for the cross-flow around four cylinders in an in-line square configuration," *J. Mech. Sci. Technol.* **21**(9), 1338 (2007).
- ¹⁹K. Lam, W. Q. Gong, and R. M. C. So, "Numerical simulation of cross-flow around four cylinders in an in-line square configuration," *J. Fluids Struct.* **24**(1), 34–57 (2008).
- ²⁰K. Lam and L. Zou, "Three-dimensional numerical simulations of cross-flow around four cylinders in an in-line square configuration," *J. Fluids Struct.* **26**(3), 482–502 (2010).
- ²¹F. Tong, L. Cheng, M. Zhao, T. Zhou, and X.-b. Chen, "The vortex shedding around four circular cylinders in an in-line square configuration," *Phys. Fluids* **26**(2), 024112 (2014).
- ²²Z. Han, D. Zhou, X. Gui, and J. Tu, "Numerical study of flow past four square-arranged cylinders using spectral element method," *Comput. Fluids* **84**, 100–112 (2013).
- ²³G. Karniadakis and S. Sherwin, *Spectral/hp Element Methods for Computational Fluid Dynamics* (Oxford University Press, 2013).
- ²⁴C. D. Cantwell, D. Moxey, A. Comerford, A. Bolis, G. Rocco, G. Mengaldo, D. De Grazia, S. Yakovlev, J.-E. Lombard, D. Ekelschot *et al.*, "Nektar++: An open-source spectral/hp element framework," *Comput. Phys. Commun.* **192**, 205–219 (2015).
- ²⁵H. Xu, C. D. Cantwell, C. Monteserin, C. Eskilsson, A. P. Engsig-Karup, and S. J. Sherwin, "Spectral/hp element methods: Recent developments, applications, and perspectives," *J. Hydron.* **30**(1), 1–22 (2018).
- ²⁶G. E. Karniadakis, M. Israeli, and S. A. Orszag, "High-order splitting methods for the incompressible Navier-Stokes equations," *J. Comput. Phys.* **97**(2), 414–443 (1991).
- ²⁷A. Miliou, S. J. Sherwin, and J. M. R. Graham, "Wake topology of curved cylinders at low Reynolds numbers," *Flow, Turbul. Combust.* **71**(1–4), 147–160 (2003).
- ²⁸H. Jiang, L. Cheng, F. Tong, D. Scott, and H. An, "Stable state of mode a for flow past a circular cylinder," *Phys. Fluids* **28**(10), 104103 (2016).
- ²⁹G. Rocco and S. J. Sherwin, "The role of spanwise forcing on vortex shedding suppression in a flow past a cylinder," in *Instability and Control of Massively Separated Flows* (Springer, 2015), pp. 105–110.
- ³⁰F. Tong, L. Cheng, C. Xiong, S. Draper, H. An, and X. Lou, "Flow regimes for a square cross-section cylinder in oscillatory flow," *J. Fluid Mech.* **813**, 85–109 (2017).
- ³¹R. Wang, Y. Bao, D. Zhou, H. Zhu, H. Ping, Z. Han, D. Serson, and H. Xu, "Flow instabilities in the wake of a circular cylinder with parallel dual splitter plates attached," *J. Fluid Mech.* **874**, 299–338 (2019).
- ³²T. Yan, R. Wang, Y. Bao, D. Zhou, H. B. Zhu, H. Ping, Z. L. Han, and B. F. Ng, "Modification of turbulent wake characteristics by two small control cylinders at a subcritical Reynolds number," *Phys. Fluids* **30**(10), 105106 (2018).
- ³³G. E. Karniadakis, "Spectral element-Fourier methods for incompressible turbulent flows," *Comput. Methods Appl. Mech. Eng.* **80**(1–3), 367–380 (1990).
- ³⁴C. J. Doolan, "Flat-plate interaction with the near wake of a square cylinder," *AIAA J.* **47**(2), 475–479 (2009).
- ³⁵A. Shankar, C. Norberg, and L. Davidson, "Simulation of three-dimensional flow around a square cylinder at moderate Reynolds numbers," *Phys. Fluids* **11**(2), 288–306 (1999).
- ³⁶D.-H. Yoon, K.-S. Yang, and C.-B. Choi, "Three-dimensional wake structures and aerodynamic coefficients for flow past an inclined square cylinder," *J. Wind Eng. Ind. Aerodyn.* **101**, 34–42 (2012).
- ³⁷G. Agbaglah and C. Mavriplis, "Computational analysis of physical mechanisms at the onset of three-dimensionality in the wake of a square cylinder," *J. Fluid Mech.* **833**, 631–647 (2017).
- ³⁸H. Jiang, L. Cheng, and H. An, "Three-dimensional wake transition of a square cylinder," *J. Fluid Mech.* **842**, 102–127 (2018).
- ³⁹D. Park and K.-S. Yang, "Flow instabilities in the wake of a rounded square cylinder," *J. Fluid Mech.* **793**, 915–932 (2016).
- ⁴⁰M. Carini, F. Giannetti, and F. Auteri, "On the origin of the flip-flop instability of two side-by-side cylinder wakes," *J. Fluid Mech.* **742**, 552–576 (2014).
- ⁴¹A. Sau, T.-W. Hsu, and S.-H. Ou, "Three-dimensional evolution of vortical structures and associated flow bifurcations in the wake of two side-by-side square cylinders," *Phys. Fluids* **19**(8), 084105 (2007).
- ⁴²G. J. Sheard, M. C. Thompson, K. Hourigan, and T. Leweke, "The evolution of a subharmonic mode in a vortex street," *J. Fluid Mech.* **534**, 23–38 (2005).